Available online at www.sciencedirect.com

jmr&t Journal of Materials Research and Technology

journal homepage: www.elsevier.com/locate/jmrt

Original Article

Laser surface alloying of copper with Cr/Ti/CNT for enhancing surface properties

Y.W. Yang [a], V.A.M. Cristino [a], L.M. Tam [a,b], K.H. Lo [a,c], C.T. Kwok [a,c,*]

[a] Department of Electromechanical Engineering, University of Macau, Macao, China
[b] Institute for Development and Quality, Macao, China
[c] Institute of Applied Physics and Materials Engineering, University of Macau, Macao, China

ARTICLE INFO

Article history:
Received 22 October 2021
Accepted 28 December 2021
Available online 5 January 2022

Keywords:
Laser surface alloying
Composite
Hardness
Wear
Corrosion

ABSTRACT

In this study, laser surface alloying of commercially pure copper (cp Cu) with Cr/Ti and Cr/Ti/CNT was conducted using a high-power diode laser. Cu–Ti intermetallic phases were detected in the Cu/Cr matrix of the laser-alloyed specimens without CNT. While TiC was found in the Cu/Cr matrix of the laser-alloyed layers with CNT. Compared to cp Cu (60 ± 10 $HV_{0.2}$), the laser-alloyed specimens without and with CNT could achieve hardness up to 423 ± 12 $HV_{0.2}$ and 860 ± 24 $HV_{0.2}$ respectively. Sliding wear tests were also carried out at 60 km/h in dry condition with a pin-on-disc tribometer. Compared with cp Cu, the wear resistances of all laser-alloyed specimens were significantly improved due to solid solution alloying, existence of harder phases including Cr, Cu–Ti intermetallics and TiC. The wear resistance of the laser-alloyed specimens was increased up to a factor of 1220 times as compared with cp Cu. For the polarization study, the corrosion current densities of all laser-alloyed specimens (0.164–0.275 μA/cm^2) in 3.5% NaCl solution at 25 °C were found to be lower than that of copper (3.362 μA/cm^2) due to presence of passive Cr and Ti.

1. Introduction

Owing to its high thermal and electrical conductivities, good ductility, and excellent atmospheric corrosion resistance, copper (Cu) has been widely used as the bearing, bushes, electrical sliding contacts and resistance welding electrodes. However, its hardness and wear resistance are relative low. In order to enhance the hardness and wear resistance of Cu, surface protection is necessary. Laser surface alloying (LSA) is a method using a high-energy laser beam to produce an alloyed layer on a substrate material [1]. The unique features of LSA include minimal thermal effect, tailor-made surface compositions and strong metallurgical bond between the alloyed layer and the substrate [1,2]. LSA can save the precious materials while the properties of the bulk can be retained. Whereas its limitations include susceptibility to cracking and formation of porosity in some alloy systems, and need of overlapping of successive alloyed tracks [3]. The properties and microstructures of the laser-alloyed layers are dependent on the selection of the alloying elements and compositional distribution. In fact, LSA of Cu is very challenging due to its low absorptivity of laser energy and high thermal

* Corresponding author.
E-mail address: fstctk@um.edu.mo (C.T. Kwok).
https://doi.org/10.1016/j.jmrt.2021.12.129

conductivity. It was reported that LSA of Cu with Cr was fabricated by preplacing and irradiation of Cr powder on the Cu substrate using a 2.5-kW CO_2 laser [4]. Their hardness and wear resistance at elevated temperature were found to be significantly improved but the electrical properties were unaffected [4]. Owing to the limited solid solubility of Cr in Cu, Cr particles were randomly dispersed in the Cu-matrix of the alloyed zone after rapid solidification. The hardness was found to be increased from 65 HV to 120 HV. On the other hand, Kwok's group reported that the hardness, electrical erosion and corrosion resistances of laser-fabricated cp Cu with different metals and alloys including W [5,6], Ti [7,8], NiTi [9,10] using a 2.3-kW diode laser were found to be improved significantly. As a matter of fact, the solid solubilities of Cr in Cu and Ti in Cu are limited to 1.56 wt.% (at 1076 °C) and 5.8 wt.% (at 900 °C) respectively, and their solubilities at room temperature are even lower, i.e. <0.03 wt.% and 0.4 wt.% respectively [11]. However, the solid solubility of the alloying elements can be extended because of rapid quenching from liquid phase [1]. Sun and his co-workers have investigated the fabrication of $Cu_{71-X}Cr_{29}Ti_X$ alloys with Ti content up to 3% using induction melting followed by rapid solidification [12]. It was found that adding Ti could partially suppress separation of the liquid phase of the molten alloy, leading to refinement of Cr-rich phase during rapid cooling. As the Ti content reached 2.5 wt.%, nano-sized intermetallic phases (Cr_2Ti and Cu_4Ti) were precipitated in the annealed alloys. Large positive mixing heat between Cu and Cr was decreased by adding Ti, resulting in separation of the liquid phase at a lower temperature driven by a smaller force. Moreover, Chai and his co-workers reported that LSA of pure Zr and pure Ti with Cr could effectively increase their surface hardness by 2.4–2.5 times those of the matrice [13,14]. The hardening effect were mainly attributed to solid-solution strengthening of Cr in pure Zr and pure Ti and significant grain refinement.

On the other hand, the protective coatings against wear may contain carbides, borides, oxides or intermetallics as the reinforcement dispersed in the metallic matrix, which possess low density, high hardness, high wear resistance and high melting temperature. Fabrication of metallic matrix composite (MMC) coatings by adding ceramic powders often suffer from weak interfacial bonding due to poor wetting, formation of undesirable interfacial products and non-uniform distribution of the ceramic phase in the metallic matrix [15]. In order to solve such problem, the composite coatings are fabricated in-situ. In-situ formation of TiC using Ti and 5–20 wt% CNT powders via laser cladding has been reported by Savalani and his co-workers [16]. The hardness and dry sliding wear resistance of the Ti–TiC composite coatings were found to be increased with higher CNT content. Moreover, fabrication of an Al–Al_4C_3 composite using ball-milled pure Al and CNT powders with laser powder-bed-fusion additive manufacturing was reported by Aboulkhair and his co-workers [17]. It was reported that strong bond and good dispersion between CNT (with high laser absorptivity) and Al (with low laser absorptivity) allowed the energy transfer from the CNT to the Al and retained the heat longer, leading to a better melt efficiency of the material. It was also reported that using CNT as the carbon source with Cu and Ti powders could produce finer TiC particles, which considerably improved the tribological properties of the TiC–C/Cu nanocomposite through the two-step-high-energy mechanical milling and in-situ annealing [18]. Compared with graphite, using CNT as the carbon source could lead to 15% reduction in wear volume loss and 16% decrease in friction coefficient. Qiu and his co-workers reported that the (TiC–TiB_2)/Cu composites with 50 vol% TiC–TiB_2 particles were successfully fabricated by the combustion synthesis and hot press consolidation from a Cu–Ti–B_4C–Cr system [19]. With the addition of Cr up to 7 wt%, the size of the TiC–TiB_2 particles were found to be smaller than 1 μm. As the Cr content increased, the yield strength, ultimate compression strength, microhardness, and abrasive wear resistance of the composites increased but the fracture strain decreased.

In view of several beneficial effects of LSA of Cu with Cr [3] and Ti [7,8], it is worthy to study the feasibility of LSA of cp Cu with Cr–Ti without and with CNT for forming in-situ IMPs and TiC in the Cu/Cr-matrix. In the present study, the hardness, wear and corrosion resistances of the laser-alloyed coatings were evaluated. It is expected that the laser-alloyed coatings with the enhanced surface properties can be used as the electrical contact materials in the harsh environments.

2. Experimental details

2.1. *Laser surface alloying*

Commercially pure Cu (cp Cu, UNS C11000) plates were used as the substrate for LSA. The plates were cut into small specimens with dimensions of 22 mm × 19 mm x 6.3 mm. To increase surface roughness for powder adhesion and remove surface oxide, the specimens were ground with an 80-grit emery paper and cooled with water. Before powder preplacement, the specimens were degreased with ethanol and then rinsed with deionized water. The relative amounts of the powder mixture of Cr (−325 mesh), Ti (−325 mesh) and multi-wall carbon nanotube (CNT, diameter of 10–30 nm and length of 5–15 μm) are presented in Table 1. The binder, polyvinyl alcohol (4 wt.%), was mixed with the Cr/Ti and Cr/Ti/CNT powders to form a slurry. The powder slurry was preplaced on the surface of cp Cu using a paintbrush and then dried with a heating fan for 5 min. In order to make sure that the powder preplaced on cp Cu was dried, a cobalt chloride test paper was placed on the dried specimen for a minute for detecting the moisture. If moisture was absence, the test paper would remain blue in colour. The thickness of the slurry was monitored to be about 0.1 mm. Preplacing powder was used instead of feeding powder for saving the precious powder and improving the laser absorption [20–23].

Prior to LSA, the specimens were preheated to 150 °C using an electric heating plate for reducing residual stress [24]. LSA was carried out using a 2.3-kW continuous-wave high-power

Table 1 – Contents of the powder mixture.

Powder mixture	Cr (wt.%)	Ti (wt.%)	CNT (wt.%)
Cr–Ti	50	50	0
Cr–Ti-CNT	40	40	20

Table 2 – Processing parameters for LSA.

Specimen designation	Beam diameter (mm)	Power P (kW)	Scanning speed V (mm/s)	No. of preplaced layers	Average thickness of alloyed layer D (mm)	Dilution ratio DR (%)
Cu–Cr–Ti P1.5V15	2	1.5	15	1	0.90	89
Cu–Cr–Ti P1.5V20	2	1.5	20	2	0.73	72
Cu–Cr–Ti-20%CNT P1.5V15	2	1.5	15	2	0.67	70
Cu–Cr–Ti-20%CNT P1.5V20	2	1.5	20	2	0.28	29

diode laser module (Laserline, LDM 1000-1000) with a wavelength of 990 nm, a beam diameter of 2 mm at a power of 1.5 kW and different scanning speeds (15 and 20 mm/s). The laser-alloyed cp Cu with Cr/Ti and Cr/Ti/CNT are designated as Cu–Cr–Ti P1.5Vxx and Cu–Cr–Ti-20%CNT P1.5Vxx respectively, where "P1.5" stands for the laser power of 1.5 kW and "Vxx" denotes the laser scanning speed (i.e. 15 or 20 mm/s) as shown in Table 2.

To avoid oxidation during LSA, Argon was used as the shroud gas flowing to the surface of the specimens at a rate of 15 L/min though a side nozzle with a inner diameter of 3 mm. The distance and angle between the nozzle and the substrate surface were 2 mm and 45° respectively. Alloying of the entire surface was completed by overlapping the successive parallel tracks with an overlapping ratio of 50%. Only one preplaced layer of Cr–Ti powders was used to fabricate the laser-alloyed specimen Cu–Cr–Ti P1.5V15 (Table 2).

In order to further increase the content of the alloying elements, a second 0.1-mm layer of the same powder mixture was preplaced on the top of previously the alloyed layer and dried with the heating fan. Two preplaced layers of the powder mixture were used to fabricate the laser-alloyed specimens including Cu–Cr–Ti P1.5V20, Cu–Cr–Ti-20%CNT P1.5V15 and Cu–Cr–Ti-20%CNT P1.5V20 (Table 2). As the surface of the first laser-alloyed layer was oxidized and undulating, it was lightly ground with the 80-grit emery paper, cooled with water, degreased with ethanol and then rinsed with deionized water. The LSA process was then repeated. The dilution ratio (DR) or degree of dilution of alloying elements in the layer, is defined as follows:

$$DR = \left(1 - \frac{t}{D}\right) \times 100\% \quad (1)$$

where t is the total thickness of the preplaced powder (i.e. 0.1 mm or 0.2 mm) and D is thickness of the alloyed layer (Table 2).

2.2. *Microstructural analysis and hardness measurement*

Microstructure and compositions of the cross-sections of the laser-alloyed specimens were analyzed using a scanning electron microscope (SEM, Hitachi S–3400N) equipped with an energy dispersive X-ray spectrometer (EDX, Horiba EX-250).

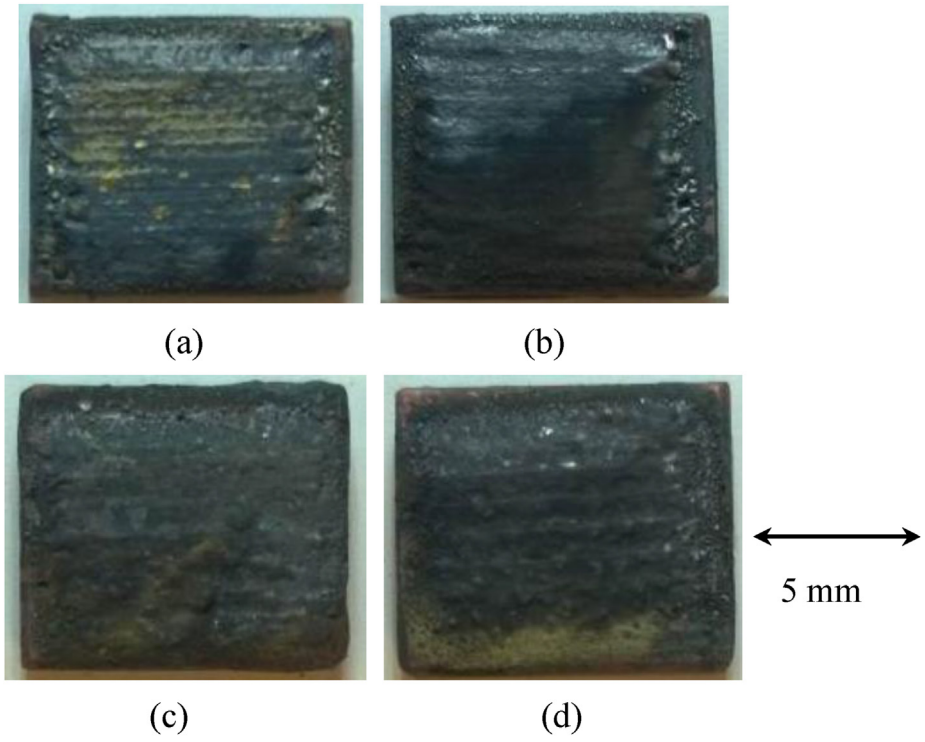

Fig. 1 – Overall top views of laser-alloyed specimens without CNT (a) Cu–Cr–Ti P1.5V15; (b) Cu–Cr–Ti P1.5V20; and with CNT (c) Cu–Cr–Ti-20%CNT P1.5V15 and (d) Cu–Cr–Ti-20%CNT P1.5V20.

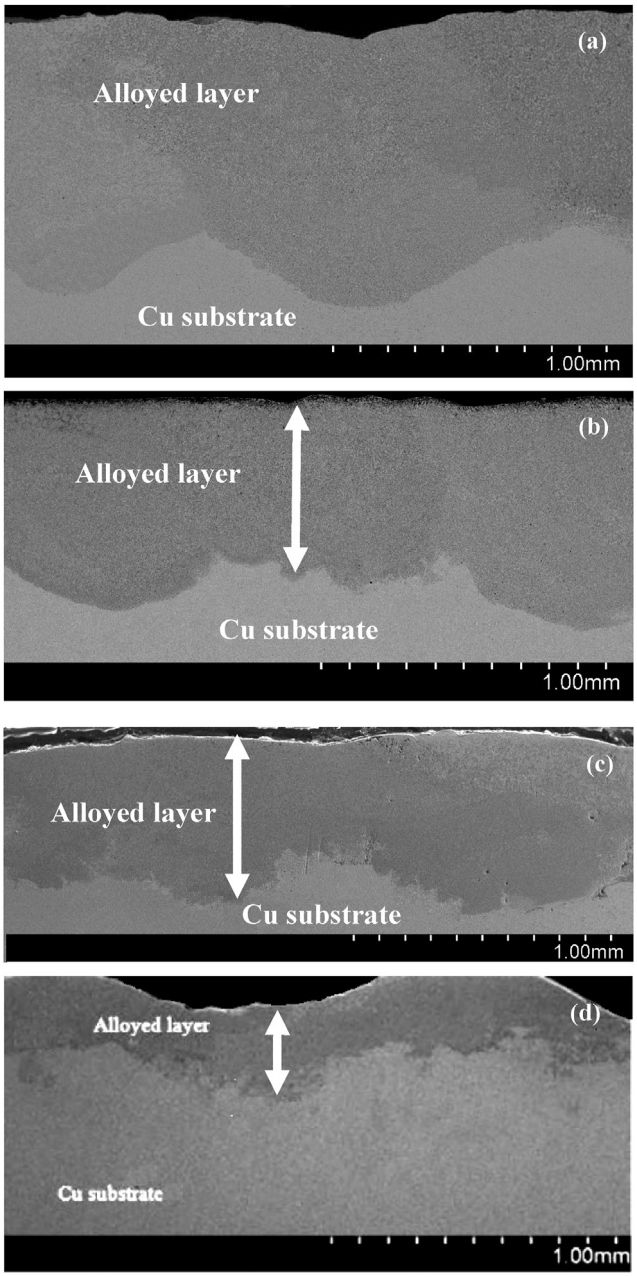

Fig. 2 – Cross-sectional views of laser-alloyed specimens without CNT (a) Cu–Cr–Ti P1.5V15; (b) Cu–Cr–Ti P1.5V20; and specimens with CNT (c) Cu–Cr–Ti-20%CNT P1.5V15 and (d) Cu–Cr–Ti-20%CNT P1.5V20.

The phases present in the surface of the laser-alloyed specimens were detected using a X-ray diffractometer (XRD, Rigaku MiniFlex 600) with CuK_{α} radiation operated at 40 kV and 15 mA with a scan rate of 0.1°/s. Average hardness along the depth of the laser-alloyed zones was measured (at least five different locations were selected) using a Vickers hardness tester with a load of 0.2 kg and a dwelling time of 10 s.

2.3. Sliding wear test

Experimental setup of sliding wear test for the laser-alloyed specimens and cp Cu in air at 25 °C using a pin-on-disc tribometer has been described in elsewhere [6,7,9,10]. During the wear test, the relative humidity was 60%. Prior to the wear test, the specimen surfaces (with an area of 22 × 19 mm^2) were polished with the 1-μm diamond paste and cleaned with ethanol. A specimen fixed in the specimen holder under a normal load of 50 N was forced to slide against at the periphery of a counterface of the rotating disc with a radius of 210 mm. The tool steel disc with a hardness of 600 $HV_{0.2}$ was selected and comparable to that of the laser-alloyed specimens. The disc was driven by an electrical motor and the specimens moved at a linear (sliding) speed of 60 km/h. The total sliding distances for the laser-alloyed specimens and cp Cu were 20 km and 1 km respectively.

The weight loss (ΔW, g) of the specimens was intermittently recorded at a time interval of 1 min using an electronic balance with an accuracy of ±0.1 mg. To ensure the repeatability of the measured data, all tests were repeated at least thrice under the same testing conditions. The standard deviation was about 5.2%. The average volume loss (ΔV, cm^3) was calculated by:

$$\Delta V = \frac{\Delta W}{\rho} \tag{2}$$

where ρ (g/cm^3) is the density of the laser-alloyed layers or cp Cu. The densities of the laser-alloyed layers were calculated using the weight fractions of Cu, Cr, Ti and TiC by the rule of mixture:

$$\frac{1}{\rho} = \frac{W_{Cu}}{\rho_{Cu}} + \frac{W_{Cr}}{\rho_{Cr}} + \frac{W_{Ti}}{\rho_{Ti}} + \frac{W_{TiC}}{\rho_{TiC}} \tag{3}$$

where ρ_{Cu} = 8.94 g/cm^3, ρ_{Cr} = 7.19 g/cm^3, ρ_{Ti} = 4.51 g/cm^3 and ρ_{TiC} = 4.94 g/cm^3 are the densities of Cu, Ni, Ti and TiC respectively. The weight fractions of Cu, Cr, Ti and TiC in the laser-alloyed layer are W_{Cu}, W_{Cr}, W_{Ti} and W_{TiC} respectively ($W_{Cu} + W_{Cr} + W_{Ti} + W_{TiC} = 1$).

The average wear rates of the specimens were calculated by the following equation:

$$\text{Wear ratexa0}(\text{mm}/\text{h}) = \frac{10 \cdot \Delta W}{\rho \cdot A \cdot \Delta t} = \frac{10 \cdot \Delta V}{A \cdot \Delta t} \tag{4}$$

where A (cm^2) is the exposed area of the specimen and Δt (h) is the duration of the wear test.

2.4. Electrochemical measurement

The laser-alloyed specimens and cp Cu with a surface area of 15 × 15 mm^2 were embedded in hot-mount resin and then polished with the 1-μm diamond paste. The gap between the specimen and the mount was sealed with epoxy resin for avoiding crevice corrosion and a surface area of 1 cm^2 was exposed. The specimens were degreased with ethanol and then rinsed with deionized water before the electrochemical measurement. Potentiodynamic polarization was performed using an electrochemical workstation (PAR, VersaSTAT3) controlled by a personal computer conforming to ASTM Standard G5-92 [25]. The test solution was 3.5 wt.% NaCl solution (open to air) and kept in an electronic water bath at 25 ± 1 °C. The reference electrode was the saturated calomel electrode (SCE, 0.244 V versus SHE at 25 °C) for potential measurement. While the counter electrode was a pair of

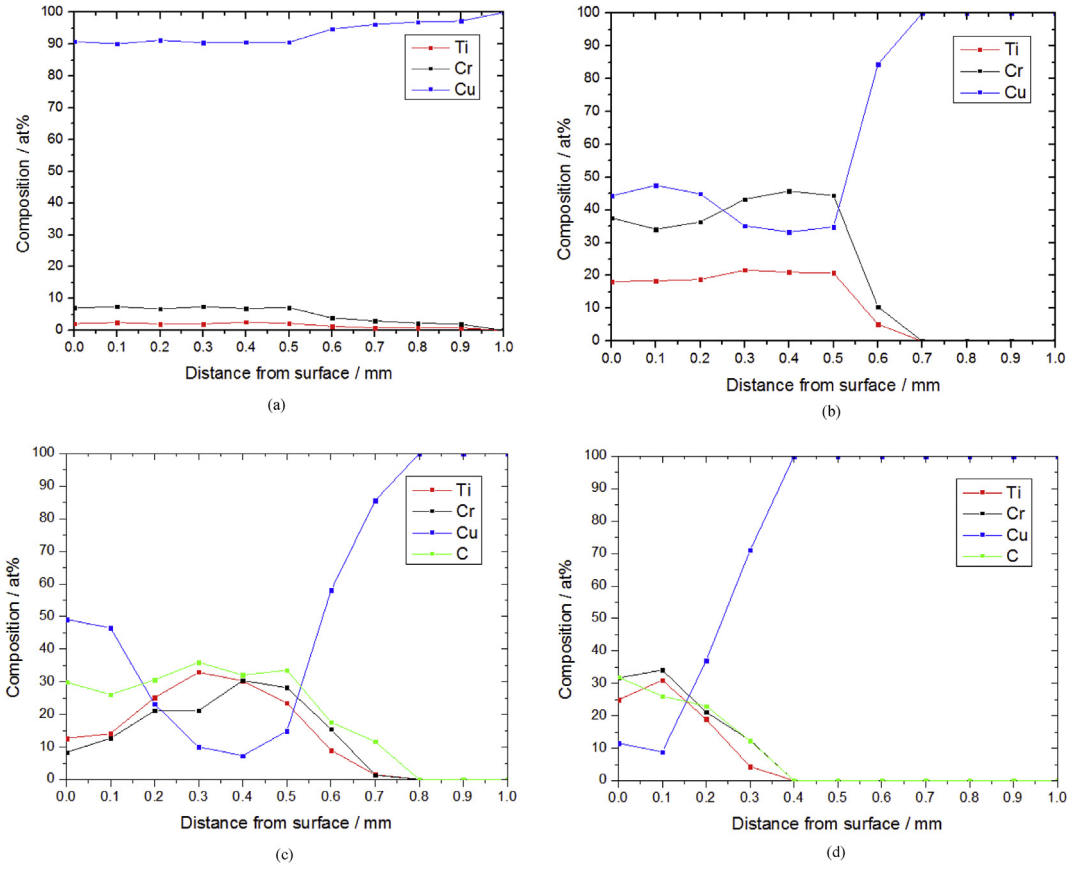

Fig. 3 – Compositional profiles of laser-alloyed specimens without CNT (a) Cu–Cr–Ti P1.5V15; (b) Cu–Cr–Ti P1.5V20; and specimens with CNT (c) Cu–Cr–Ti-20%CNT P1.5V15 and (d) Cu–Cr–Ti-20%CNT P1.5V20.

graphite rods for measuring the current. After an initial delay for 5 min, the potential was increased at a rate of 0.167 mV/s, starting from 0.2 V_{SCE} below the free corrosion potential. Corrosion potential (E_{corr}) and corrosion current density (I_{corr}) were extracted from the polarization curve using Tafel extrapolation method with the software (PowerCORR, V.2.42). Three replicas were taken for the electrochemical test for each specimen.

3. Results and discussion

3.1. *Microstructural and metallographic analyses*

The overall top views, cross-sections and compositional profiles of the laser-alloyed Cu with Cr/Ti (without CNT) and Cr/Ti/CNT are shown in Fig. 1, Fig. 2 and Fig. 3 respectively. All laser-alloyed layers were metallurgically bonded on the cp Cu substrate without crack and porosity (Fig. 2). The average thicknesses of the alloyed zones are found to be in the range of 0.24–0.90 mm (Table 2). The average thickness of the laser-alloyed layer increases with the decrease in the scanning speed. For the laser-alloyed specimen without CNT processed with a lower scanning speed (i.e. Cu–Cr–Ti P1.5V15), the thickness of the alloyed layer is larger, the Cr and Ti contents are lower and the *DR* is higher (78%). Whereas, the laser-alloyed specimen without CNT fabricated at higher scanning speed (i.e. Cu–Cr–Ti P1.5V20) possesses higher Cr and Ti contents and lower *DR* (Fig. 3 and Table 2). On the other hand, the thickness of the alloyed zones of the laser-alloyed specimens with CNT are shallower than the ones without CNT as shown in Fig. 2c-d. The specimen surfaces are corrugated. The average compositions of the laser-alloyed specimens are given in Table 3. From the XRD patterns (Fig. 4a and b), Cu, Cr and intermetallic phases (IMPs) (Cu_3Ti, Cu_3Ti_2, Cu_4Ti_3) were detected in the laser-alloyed specimens without CNT. While Cu, Cr and TiC were found in the laser-alloyed specimens with CNT (Fig. 4c and d).

During laser irradiation on the specimens preplaced with the Cr and Ti powders (without CNT), the powders melted instantaneously. The superficial cp Cu was also melted because the heat from the molten powders was conducted to cp Cu substrate. With the large temperature gradient (100–10,000 K/mm) between the center of the melt pool and the cooler solid–liquid interface [26] and surface tension, Marangoni fluid flow could lead to mixing of the molten elements in the alloyed zones. For the laser-alloyed specimen without CNT processed at a lower scanning speed (Cu–Cr–Ti P1.5V15), the Cr particles with a darker contrast are observed in the Cu-matrix with brighter contrast (Fig. 5a). The major

Table 3 – Compositions of and phases present in various specimens.

Specimen	Average composition of alloyed layer (wt%)				Major phases	Minor phases
	Cu	Cr	Ti	C		
cp Cu	100	0	0	–	Cu	–
Cu–Cr–Ti P1.5V15	91.0	6.6	2.4	–	Cu	Cr, Cu_3Ti
Cu–Cr–Ti P1.5V20	44.2	37.6	18.2	–	Cu	Cr, Cu_3Ti, Cu_3Ti_2, Cu_4Ti_3
Cu–Cr–Ti-20%CNT P1.5V15	35.6	26.5	29.0	8.9	Cu	Cr, TiC
Cu–Cr–Ti-20%CNT P1.5V20	13.5	43.0	35.9	7.6	Cr	TiC, Cu

phase Cu-matrix is reinforced with Cr and Cu_3Ti as the minor phases (Fig. 4a). As the solubility of Cr in Cu is limited, the undissolved Cr particles (indicated by 'B') with average size of 1 μm are uniformly dispersed in the Cu-matrix (indicated by 'A') as shown in Fig. 5a. From the BSE micrograph of the laser-alloyed specimen without CNT processed at higher scanning speed (Cu–Cr–Ti P1.5V20) (Fig. 5b), three distinct phases with different contrast [light grey (indicated by A), grey (indicated by B) and dark grey (indicated by C)] are observed and their compositions are also shown in the table. Clusters of the phases were randomly dispersed in the alloyed layers. The microstructure was quite heterogeneous as the Cr and Ti contents were higher resulting in forming more Cr-rich (grey) and Cu–Ti IMPs (dark grey) in the alloyed layers. From Fig. 4b, Cu is the major phase with the IMPs (Cu_3Ti, Cu_3Ti_2, and Cu_4Ti_3) are the minor phases.

For the laser-alloyed specimen with CNT fabricated at lower scanning speed (Cu–Cr–Ti-20%CNT P1.5V15), two types of reinforcement [i.e. Cr particles (36 vol%) and dendritic TiC (20.4 vol%] are present in the Cu-matrix (43.6 vol%) as shown in Fig. 6a. The average sizes of the Cr particles and TiC dendrites in Cu–Cr–Ti-20%CNT P1.5V15 are found to be 3.5 and 1.6 μm respectively [Fig. 6a(ii)]. For the one fabricated at higher scanning speed (Cu–Cr–Ti-20%CNT P1.5V20), on the contrary, the high content of dendritic TiC (60.5 vol%) is dispersed in the Cr-matrix as shown in Fig. 6b, and a small amount of Cu phase is inevitably mixed into the Cr-matrix. The average size of the dendritic TiC in Cu–Cr–Ti-20%CNT P1.5V20 is 3.4 μm [Fig. 6b(ii)]. Compared with Cu–Cr–Ti-20%CNT P1.5V15, Cu–Cr–Ti-20%CNT P1.5V20 possessed more and larger TiC dendrites because the shorter interaction time led to lower degree of dilution (i.e. higher Ti and C contents) in the laser-

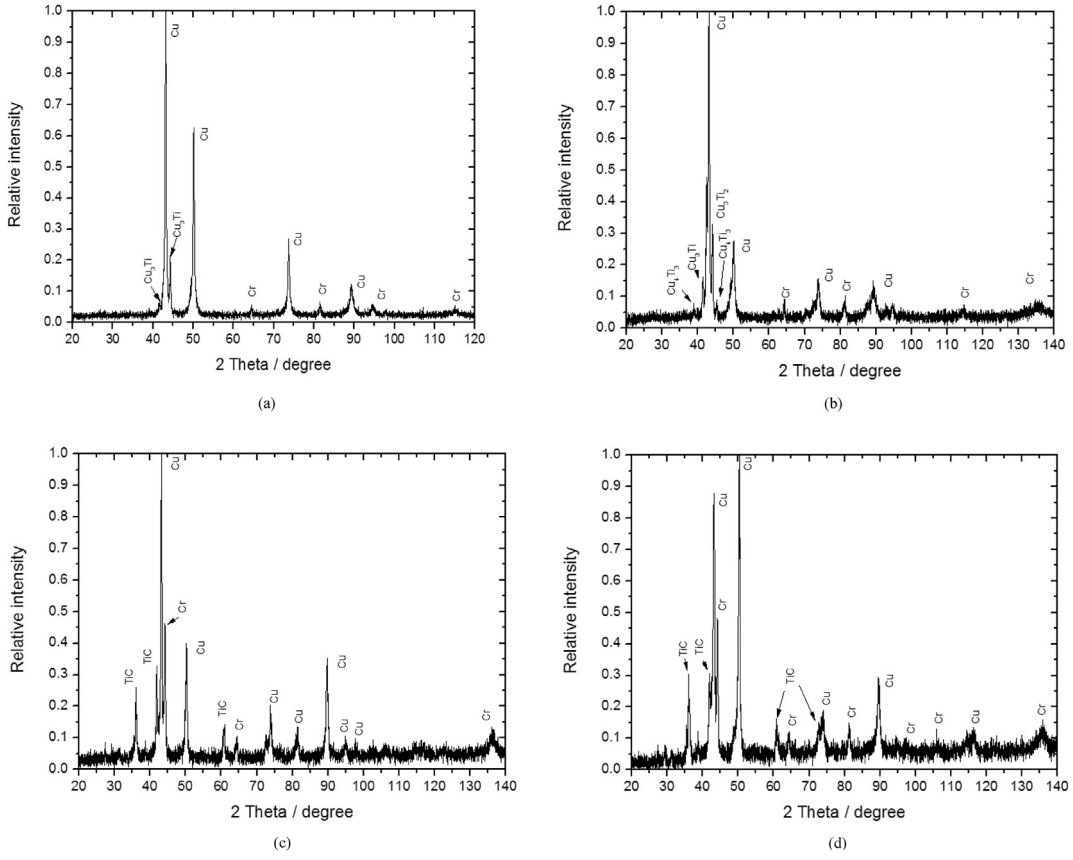

Fig. 4 – XRD spectra of laser-alloyed specimens without CNT (a) Cu–Cr–Ti P1.5V15; (b) Cu–Cr–Ti P1.5V20; and specimens with CNT (c) Cu–Cr–Ti-20%CNT P1.5V15 and (d) Cu–Cr–Ti-20%CNT P1.5V20.

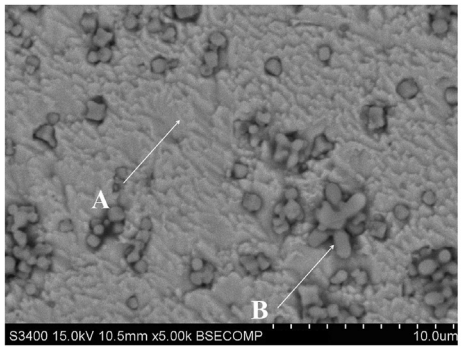

Composition	Ti (wt.%)	Cr (wt.%)	Cu (wt.%)
A (Cu-rich, 83.6 vol%)	3.2	1.5	95.3
B (Cr-rich, 16.4 vol%)	3.8	88.1	8.1

(a)

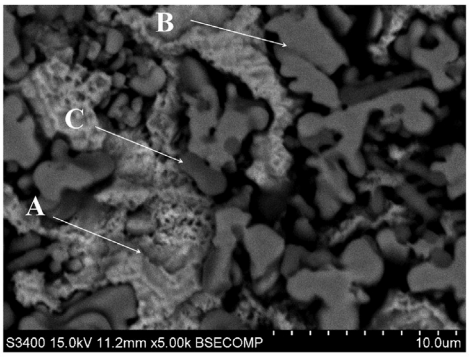

Composition	Ti (wt.%)	Cr (wt.%)	Cu (wt.%)
A (Cu-rich, 32.9 vol%)	3.9	2.8	94.3
B (Cr-rich, 28.2 vol%)	4.3	94.2	1.5
C (Ti-rich, 8.3 vol%)	51.6	35.5	12.9

(b)

Fig. 5 – BSE micrographs of laser-alloyed specimens without CNT (a) Cu–Cr–Ti P1.5V15; and (b) Cu–Cr–Ti P1.5V20.

alloyed zone. The SEM micrographs show no evidence of interfacial delamination or debonding at the interfaces of the various phases. From the contiguous microstructure of Cu-matrix or Cr-matrix contacted with TiC (Fig. 6), the EDX line scans across three phases including TiC, Cu and Cr in the alloyed zones of the laser-alloyed specimens reveal the relative amount of Cu, Cr, Ti and C as shown in Fig. 6a(ii)-(iii) and Fig. 6b(ii)-(iii). From the compositions as shown in the tables of Fig. 6, the phase 'A' is rich in Cu, while the phase 'B' is rich in Cr and the phase 'D' mainly contains Ti with C corresponding to the phases Cu, Cr and TiC respectively. However, no CNT was detected in the XRD patterns of the laser-alloyed specimens (Fig. 4d-e) because the CNT was decomposed and carbon was combined with Ti as TiC. Wang and co-workers [27] also reported that CNT was not detected in the XRD pattern of the selective-laser-melted AlSi10Mg due to decomposition of CNTs and dissolution of carbon into the Al-matrix. Moreover, Ti possesses a more negative heat of formation with carbon (−184.0 J/mol) than that of Cr with carbon in molten state [28]. This indicated that Ti and carbon had a larger driving force to form TiC. The mechanism for the evolution of in-situ Cu–Cr–TiC or Cr–Cu–TiC composites during LSA is depicted in Fig. 7. During LSA, concentration gradient and temperature gradient at solid/liquid interface could lead to Marangoni flow in the melt pool surface and capillary forces in the pool (Fig. 7b). As the laser beam irradiated on the powder mixture, the capillary forces generated the torques around the CNTs resulting in redistribution (Fig. 7b). The absorptivities of Cu, Cr, Ti and CNT at 990 nm (for the diode laser used in this study) are 9% [29], 37% [30], 65% [29] and 82% [31] respectively. As the absorptivity of laser energy of the CNTs is the highest, the temperature of the CNT and its surrounding was much higher than the average temperature of the melt pool, and interfacial reaction was easily initiated. Compared with Cu and Cr, the laser energy can be easily absorbed by the CNT and Ti during LSA due to their higher absorptivities of the laser [27,29–32]. Under Ar shielding, decomposition of the CNT occurred above 2800 °C under the irradiation of the laser beam [33] (Fig. 7c). The CNT was dissociated and the carbon atoms were combined with Ti in the melt pool as the TiC. Hence, the TiC dendrites were dispersed in the Cu-matrix (Cu–Cr–Ti-20% CNT P1.5V15) or Cr-matrix (Cu–Cr–Ti-20%CNT P1.5V20) as the composite after rapid solidification (Fig. 7d).

3.2. *Hardness*

The hardness profiles along the depth of various laser-alloyed specimens are shown in Fig. 8. The maximum hardness of the alloyed layers are summarized in Table 4. The hardness of all laser-alloyed layers are much higher than that of cp Cu (60 ± 10 $HV_{0.2}$). Owing to their lower Ti content, the hardness values of Cu–Cr–Ti P1.5V15 (271 ± 12 $HV_{0.2}$) and Cu–Cr–Ti P1.5V20 (423 ± 12 $HV_{0.2}$) are lower than that of the laser-alloyed Cu with 70 wt.% Ti (LA-Ti-Cu-20, 661 ± 41 $HV_{0.2}$) [7,8]. The enhanced hardness of the laser-alloyed specimen without CNT processed at a lower scanning speed (Cu–Cr–Ti P1.5V15) with high *DR* is due to solid solution hardening of Cu with Ti, and dispersion hardening of Cr and Cu_3Ti. For the laser-alloyed specimen without CNT processed at a higher scanning speed, the increase in hardness is mainly attributed to presence of the hard IMPs (Cu_3Ti, Cu_3Ti_2, Cu_4Ti_3) and Cr phase.

For the laser-alloyed specimens with CNT, the hardness of Cu–Cr–Ti-20%CNT P1.5V20 was achieved to 860 ± 25 $HV_{0.2}$ but the hardness of Cu–Cr–Ti-20%CNT P1.5V15 is lower (595 ± 18 $HV_{0.2}$) owing to presence of more and larger TiC in the former. Under the same laser processing condition, the laser-alloyed specimen with CNT (Cu–Cr–Ti-20%CNT P1.5V20) is harder than the one without CNT (Cu–Cr–Ti P1.5V20, 423 ± 12 $HV_{0.2}$) (differs by a factor of 2).

3.3. *Wear behavior*

The plot of cumulative volume loss versus wear distance for the laser-alloyed specimens and cp Cu in air are shown in

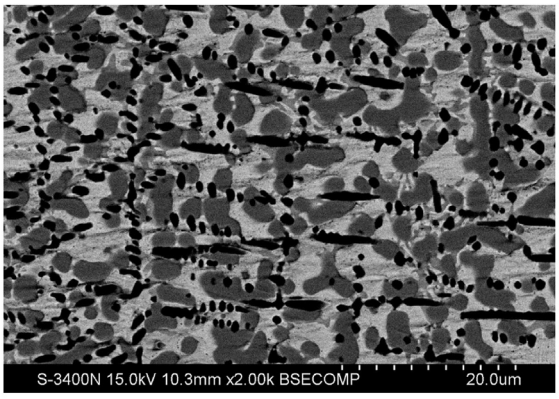

(a)(i)

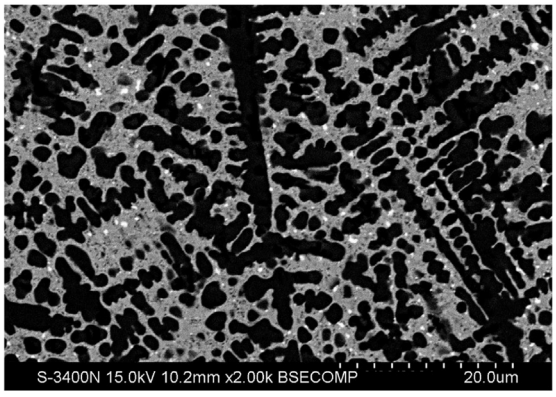

(b)(i)

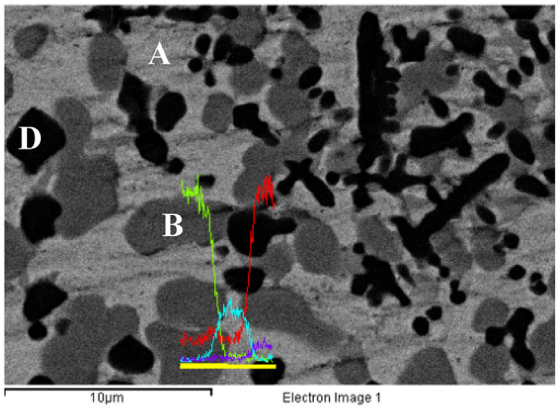

(a)(ii)

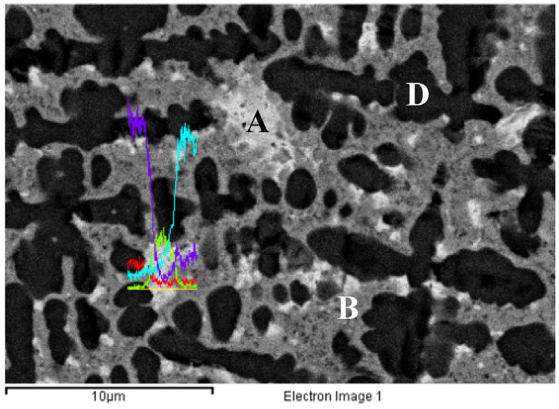

(b)(ii)

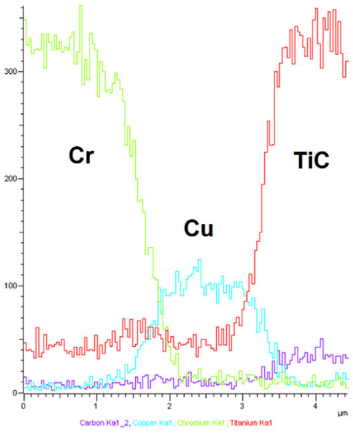

Composition	C (wt.%)	Ti (wt.%)	Cr (wt.%)	Cu (wt.%)
A (Cu-rich, 43.6 vol%)	0	7.3	1.8	90.9
B (Cr-rich, 36 vol%)	0	7.2	90.6	2.2
D (TiC, 20.4 vol%)	16.9	71.6	5.0	6.5

(a)(iii)

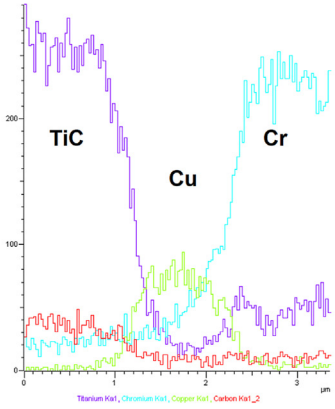

Composition	C (wt.%)	Ti (wt.%)	Cr (wt.%)	Cu (wt.%)
A (Cu-rich, 5.6 vol-%)	0	2.1	7.2	90.7
B (Cr-rich, 33.9 vol-%)	0	9.9	85.0	5.1
D (TiC, 60.5 vol-%)	16.8	74.6	8.6	0

(b)(iii)

Fig. 6 – Laser-alloyed specimens with CNT (a) Cu–Cr–Ti-20%CNT P1.5V15 and (b) Cu–Cr–Ti-20%CNT P1.5V20: (i) BSE micrograph with low magnification; (ii) BSE micrograph with high magnification; and (iii) EDX line scan across the TiC, Cu and Cr phases.

Fig. 9 and their average wear rates are depicted in Table 4. The wear rates of the laser-alloyed specimens were much lower than that of cp Cu which was seriously worn for a wear distance of 1 km [6,7,9]. For the laser-alloyed specimens, only small volume losses (low wear rates) were detected. The ranking of wear resistance (i.e. reciprocal of wear rate) is shown below:

Cu–Cr–Ti-20%CNT P1.5V20 > Cu–Cr–Ti-20%CNT P1.5V15 > Cu–Cr–Ti P1.5V20 > Cu–Cr–Ti P1.5V15 >> cp Cu

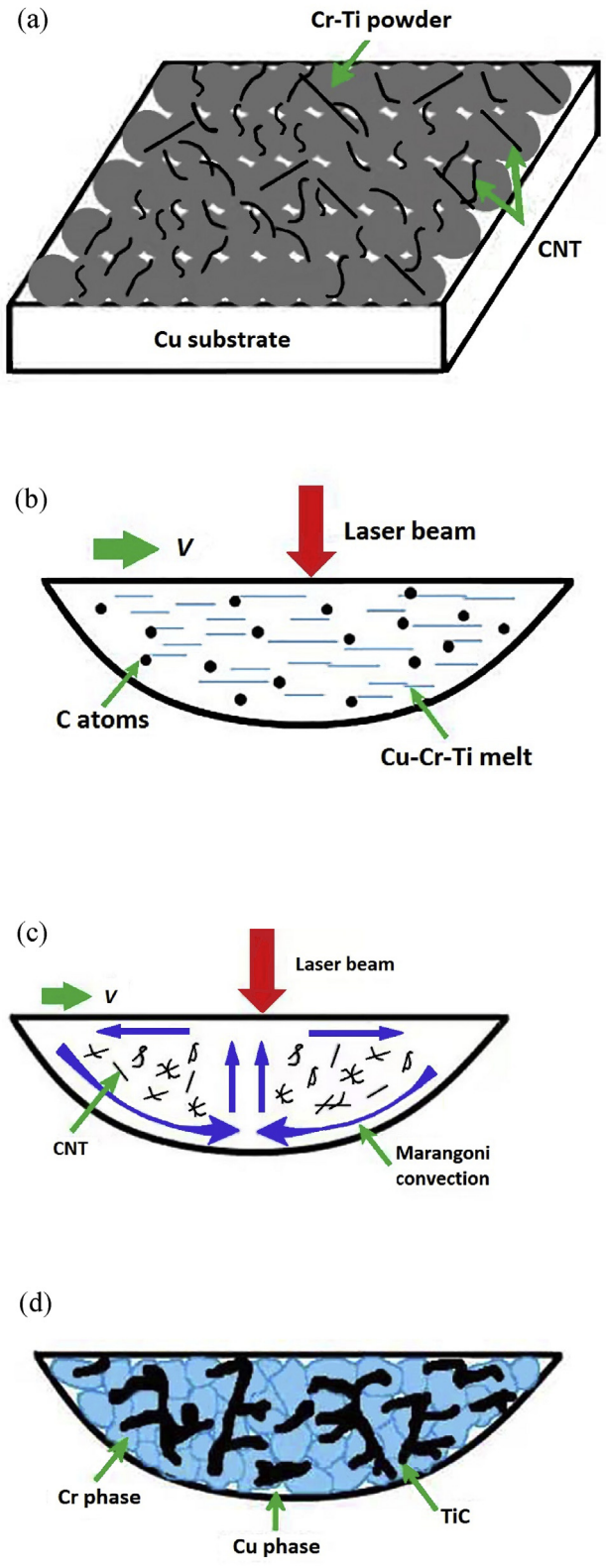

Fig. 7 – Schematic of evolution mechanism of Cr-Cu-TiC during LSA.

Among the specimens, the wear rate of Cu–Cr–Ti-20%CNT P1.5V20 is the lowest owing to the existence of high volume fraction of TiC in the hard Cr-matrix leading to a significant improvement in hardness and wear resistance. While the wear rate of Cu–Cr–Ti P1.5V15 is the highest due to the low Cr and $CuTi_3$ contents in the soft Cu-matrix. The wear resistances of the laser-alloyed specimens without CNT and with CNT are superior to that of cp Cu by 68 and 1220 times respectively.

From the previous studies of Kwok's group, the sliding wear behavior of the laser-alloyed Cu with W (60 wt%, designated as LA-W-Cu-p2) [6], with Ti (70 wt%, designated as LA-Ti-Cu-30) [7], and with NiTi (38 at% Ni, 39 at% Ti, 5 at% O, designated as LA-NiTi-Cu-35-45-45) [9] in air was reported. The ranking of wear resistance of the laser-alloyed Cu with different elements/alloy is (Table 4):

LA-NiTi-Cu-35-45-45 > Cu–Cr–Ti-20%CNT P1.5V20 > LA-W-Cu-p2 > LA-Ti-Cu-30 > > cp Cu

The wear resistance of Cu–Cr–Ti-20%CNT P1.5V20 is slightly lower than LA-NiTi-Cu-35-45-45 but higher than the other laser-alloyed specimens. It was reported that the microstructure of the laser-alloyed Cu with W contained the uniformly distributed micro-sized W particles in the Cu-matrix [7]. The improved wear resistance of the laser-alloyed Cu with W was due to the W phase with a higher hardness and a higher softening temperature, and the existence of tungsten oxide. On the other hand, the enhanced wear resistance of the laser-alloyed Cu with Ti is due to both solid-solution hardening and the hard Cu–Ti IMPs [9]. The harder IMPs in the laser-alloyed layers could reduce the load to be transferred to the softer Cu phase [34]. Besides the IMPs, the surface oxide could act as the lubricant for reducing wear. Moreover, oxide particle strengthening and composite strengthening could strengthen the laser-alloyed layers during wear [35]. On the other hand, the extraordinary wear resistant laser-alloyed Cu with NiTi is owing to pseudo-elastic effect for accommodating deformation [9]. Also, the harder IMPs could help to withstand the external load, and oxide formation and work hardening could assist in enhancing the wear resistance.

In the present study, the enhanced wear resistance of the laser-alloyed specimen without CNT (Cu–Cr–Ti P1.5V20) is mainly due to the hard Cu–Ti IMPs [7], to a lesser extent, solid solution strengthening [8]. More Cu–Ti IMPs also could lead to a higher hardness and wear resistance. Whereas the enhanced wear resistance of the laser-alloyed specimen with CNT (Cu–Cr–Ti-CNT P1.5V20) was due to the existence of higher volume fraction of TiC particles (60.5 vol%, 1033 $HV_{0.2}$) in the Cr-matrix (33.9 vol%, 540 $HV_{0.2}$) with higher hardness. Both phases possessed higher melting temperatures (Cr: 1615 °C and TiC: 3160 °C) and hence higher softening temperatures than Cu (1083 °C). While wear resistance of Cu–Cr–Ti-CNT P1.5V15 is lower because of lower volume fraction of Cr phase (36 vol%) and TiC particles (20.4%) in the higher volume fraction of softer Cu-matrix (43.6 vol%). It was reported that the wear resistance of Cu-xTiC composites (x = 10, 20 and 36%) fabricated by mechanical milling and in-situ reaction increased with increase in the volume fraction of TiC [36]. The TiC particles could bear the applied load and resist against plastic deformation of the Cu-matrix [36]. In the present study, the laser-alloyed specimen Cu–Cr–Ti-CNT

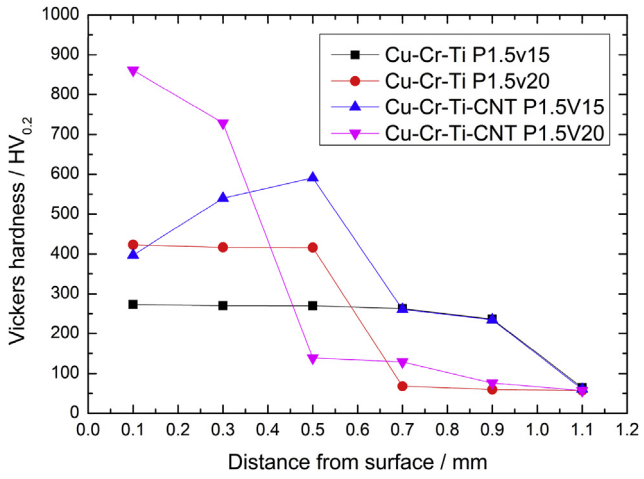

Fig. 8 – Hardness profiles along the cross-section of various specimens.

P1.5V20 with high volume fraction of TiC in the Cr-matrix greatly enhances its wear resistance. With more TiC particles, the Cr-matrix was reluctant to the movement of TiC which it held. By the Archard's law, wear resistance is directly proportional to hardness and this dependence justifies the higher wear resistant behavior that prevails in Cu–Cr–Ti-CNT P1.5V20 with higher hardness.

The SEM micrographs of the worn surfaces of the laser-alloyed specimens (Fig. 10 and Fig. 11) show that the material lost from three distinct mechanisms: (i) wear of matrix; (ii) wear of reinforcements by micro-cracking and brittle fracture; and (iii) dislodging of the reinforcements from the matrix (initiates at reinforcement/matrix interface) [37]. As no superficial and insidious cracks were observed on the surface and in the alloyed layers of the laser-alloyed specimens without and with CNT before the wear test (Figs. 2, 5 and 6), the cracks observed in the laser-alloyed specimens after the wear test (Figs. 10 and 11) were resulted from the wear test rather than the process of LSA.

From Fig. 10, many grooves parallel to the sliding direction and more severely deformed surface were observed in Cu–Cr–Ti-20%CNT P1.5V15 reflecting more serious wear damage due to its lower wear resistance (lower hardness) as compared with Cu–Cr–Ti-20%CNT P1.5V20 (Fig. 11). The grooves were made by the abrasion of the dislodged TiC/Cr particles and the harder asperities of the counterface (i.e. the disc) resulting in plastic deformation of the softer Cu-matrix. From Fig. 10b, the TiC particles with size smaller than 1 μm were found to be remained on the worn surface of Cu–Cr–Ti-20%CNT P1.5V15 as indicated by the red arrows. From the EDX results (the table in Fig. 10), high Ti and C contents were detected on the worn surface of Cu–Cr–Ti-20%CNT P1.5V15 (location H). The presence of Fe patches on the worn surfaces was due to transfer of material from the steel disc during sliding wear (location E). Also, the oxides (FeO and CuO) detected on the laser-alloyed specimens with CNT was probably due to oxidative wear (Fig. 10a). For Cu–Cr–Ti-20%CNT P1.5V15, wear commenced locally in the soft Cu-matrix and the TiC particles lost their protection from the Cu-matrix. The reinforcement (TiC) with smaller size was easily dislodged from the relative soft Cu-matrix at the interface between the reinforcement and the matrix. As the reinforcements were dislodged, free hard TiC and Cr particles could go into the contact region resulting in three-body abrasive wear which probably caused the more and deeper grooves on the weaker Cu-matrix. Compared with TiC in Cu–Cr–Ti-20%CNT P1.5V15, the volume fraction and size of the Cr particles are larger, however, its effect on the improvement in hardness is less significant.

On the contrary, no groove was observed on the surface of Cu–Cr–Ti-20%CNT P1.5V20 but transgranular micro-cracks in the TiC and Cr phases and some of Fe-rich patches adhered on the surface were observed (Fig. 11). The transgranular micro-cracks were observed across the TiC and Cr phases due to their brittleness. However, the cracked TiC and Cr phases were still remained on the worn surface of Cu–Cr–Ti-20%CNT P1.5V20. From the EDX results of as shown in the table of Fig. 11, high Ti and C contents were detected at location X, high Cr content was detected at location Y and high Fe content was detected at location Z but no oxygen were detected. It is noticed that the Fe content in Cu–Cr–Ti-20%CNT P1.5V20 is higher than that in Cu–Cr–Ti-20%CNT P1.5V15 due to the higher hardness and wear resistance of the former. More material was transferred from the softer steel disc to Cu–Cr–Ti-20%CNT P1.5V20.

Generally speaking, the improved wear resistance of the laser-alloyed specimens without and with CNT is attributed to dislocation strengthening (due to deformation), solid solution strengthening (by alloying with Cr and Ti), particle strengthening (oxide particles), and composite strengthening (existence of TiC, Cr and IMPs). Comparing both laser-alloyed specimens with CNT, it can be observed that the improvement in the wear resistance is attributed to the type, size and volume fraction of the reinforcements and also the hardness

Table 4 – Maximum hardness, wear rate, I_{corr} and E_{corr} of various specimens.

Specimen	Maximum hardness ($HV_{0.2}$)	Wear rate (mm/h)	E_{corr} vs SCE (V_{SCE})	I_{corr} (μA/cm^2)
cp Cu	60 ± 10	293.00	−0.216 ± 0.004	3.362 ± 0.061
Cu–Cr–Ti P1.5V15	271 ± 12	13.40	−0.198 ± 0.001	0.275 ± 0.011
Cu–Cr–Ti P1.5V20	423 ± 12	4.31	−0.206 ± 0.002	0.184 ± 0.006
Cu–Cr–Ti-20%CNT P1.5V15	595 ± 22	0.60	−0.170 ± 0.001	0.164 ± 0.005
Cu–Cr–Ti-20%CNT P1.5V20	860 ± 24	0.24	−0.185 ± 0.002	0.170 ± 0.007
LA-W-Cu-p2 [5,6]	150 ± 26	1.00	−0.337	1.096
LA-Ti-Cu-30 [7,8]	661 ± 41	0.99	−0.309	0.026
LA-NiTi-Cu-35-45-45 [9,10]	435 ± 43	0.08	−0.252	0.283

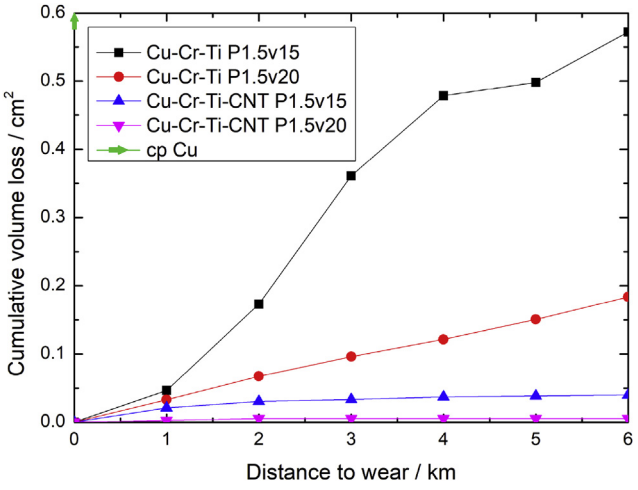

Fig. 9 – Plot of cumulative volume loss versus wear distance for various specimens.

of the matrix. For the laser-alloyed specimen processed at lower scanning speed (Cu–Cr–Ti-20%CNT P1.5V15), the reinforcements (36 vol-% Cr particles and 20.4 vol-% dendritic TiC with sizes of 3.5 and 1.6 μm respectively) are distributed uniformly in the Cu-matirx (Fig. 6a). For the one fabricated at higher scanning speed (Cu–Cr–Ti-20%CNT P1.5V20), 60.5 vol-% TiC is dispersed in the Cr-matrix with particle size of 3.4 μm. Increase in the volume fraction and size of the reinforcement (TiC particles) significantly increases the wear resistance of the laser-alloyed specimens. Moreover, the hard Cr-matrix (i.e. Cu–Cr–Ti-20%CNT P1.5V20) also plays an important role. The larger TiC particles in Cu–Cr–Ti-20%CNT P1.5V20 were retained in the matrix but micro-cracking and brittle fracture occurred, leading to partial losses of the reinforcement particles as shown in Fig. 11. Propagation of transgranular micro-crack indicates the relatively strong interphase bond between the TiC particles and Cr-matrix. In the sliding wear system, the hardness of the counterbody (i.e. the disc, 600 $HV_{0.2}$) is lower than those of the TiC particles (1033 $HV_{0.2}$) and comparable to Cr (540 $HV_{0.2}$) but higher than that of Cu (60 $HV_{0.2}$) in the laser-alloyed specimens. As the hardness of the Cu phase is much lower than that of the counterbody under the severe loading conditions, it will tend to be worn away from surface under the action of the three-body abrasion. The Cu phase in Cu–Cr–Ti-20%CNT P1.5V15 was extensively damaged (plastically deformation and scratched) and it is more susceptible to sliding wear (Fig. 10).

3.4. *Corrosion behavior*

Fig. 12 shows the potentiodynamic polarization curves of different laser-alloyed specimens and cp Cu in the 3.5 wt% NaCl solution (open to air) at 25 °C. The E_{corr} and I_{corr} are extracted from the curves as shown in Table 4. It can be seen that the values of E_{corr} of the laser-alloyed specimens without and with CNT are nobler than that of cp Cu. The I_{corr} of all laser-alloyed specimens (0.164–0.275 $\mu A/cm^2$) are lower than that of cp Cu (3.362 $\mu A/cm^2$) by an order of magnitude. Among the laser-alloyed specimens, the E_{corr} of the one with CNT containing less TiC but more Cu phase (i.e. Cu–Cr–Ti-CNT P1.5V15) is noblest due to the presence of nobler Cu phase as the matrix (43.6 vol%).

As cp Cu is not self-passivating, its I_{corr} (corrosion rate) in the 3.5 wt% NaCl solution is higher than those of the laser-alloyed specimens containing the passivable elements (i.e. Cr and Ti) (Table 4). The corrosion rates of the laser-alloyed specimens decrease as the contents of Cr and Ti increase. Based on the I_{corr} (Table 4), the corrosion resistance ranking of the laser-alloyed specimens in the 3.5 wt.% NaCl solution at 25 °C is:

Cu–Cr–Ti-20%CNT P1.5V15 ~ Cu–Cr–Ti-20%CNT P1.5V20 > Cu–Cr–Ti P1.5V20 > Cu–Cr–Ti P1.5V15 > cp Cu

The laser-alloyed specimens with CNT are the most corrosion resistant among all specimens due to the highest Cr and Ti contents (the lowest *DR*) and existence of passive oxide film. Generally speaking, increase in Cr and Ti contents in the laser-alloyed layers could reduce the I_{corr}. It was reported that dechromisation of Cu–47%Cr [38] and Cu-50.54%Cr-0.42%Ni-1.34%Al [39] in acid occurred at the interface between the Cr-rich phase and the Cu-rich phase, then extended gradually to the Cr-rich phase until it was dissolved thoroughly. In the present study, passive Cr and Ti are expected to be cathodic to Cu when exposed to the neutral 3.5 wt% NaCl solution (open to air) at 25 °C. Cu is more susceptible to chloride attack and dissolves as $CuCl_2^-$ in the NaCl solution [40].

$$Cu + Cl^- \rightarrow CuCl^- \quad (5)$$

$$CuCl^{-nbsp} + Cl^- \rightarrow CuCl_2^- \quad (6)$$

While the corrosion resistance of Cr and Ti was reflected by passivity due to the existence of protective oxides (Cr_2O_3 and TiO_2) which are stable in the aerated NaCl solution. For the laser-alloyed specimens without CNT, the Cu phase, Cr phase and the Cu–Ti IMPs were present. The partial protective oxide was formed on the Cu–Ti IMPs and the Cr phase (cathodic) present in the laser-alloyed specimens (Cu–Cr–Ti P1.5V15 and Cu–Cr–Ti P1.5V20) while the Cu-matrix (anodic) was selectively attacked. Although their I_{corr} were found to be reduced, the more active Cu phase was attacked selectively.

The E_{corr} of two laser-alloyed specimens with CNT (Cu–Cr–Ti-20%CNT P1.5V15 and Cu–Cr–Ti-20%CNT P1.5V20) are nobler than those of the ones without CNT and the laser-alloyed Cu with W [5], Ti [8] and NiTi [10] (Table 4). But both specimens do not show considerable passivity. Based on the I_{corr}, their corrosion resistance ranking in the 3.5 wt% NaCl solution is:

LA-Ti-Cu-30 > Cu–Cr–Ti-20%CNT P1.5V15 ~ Cu–Cr–Ti-20% CNT P1.5V20 > LA-NiTi-Cu-35-45-45 > LA-W-Cu-p2 > cp Cu

It is noteworthy that the laser-alloyed Cu with different metallic elements or alloy show different corrosion behavior and mechanisms [5,8,10]. It was reported that the corrosion rate of the laser-alloyed Cu with W (55–60 wt%) in the 3.5 wt.% NaCl solution decreased with the decrease in Cu content [5]. Although the laser-alloyed Cu with W did not show significant passivity and thermodynamic stability was not as noble as cp Cu, they have lower I_{corr} than that of cp Cu (improved by a

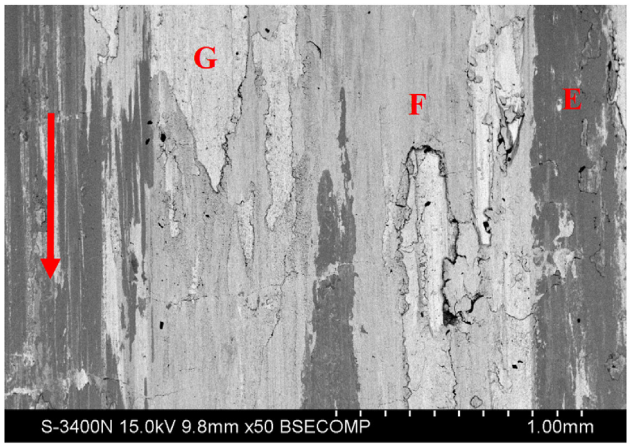

(a)

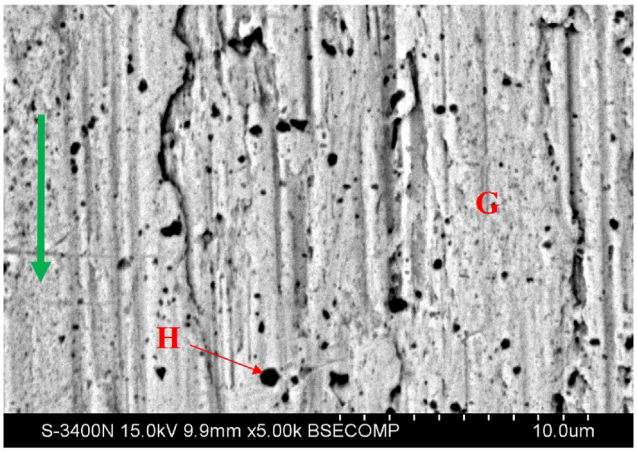

Composition (wt.%)	Ti	Cr	Fe	Cu	O	C
E (FeO)	8.8	8.7	41.7	8.6	29.6	2.6
F (CuO)	5.9	5.2	8.9	63.1	12.3	4.6
G (Cu-rich)	5.2	7.0	0.6	78.6	2.9	5.7
H (TiC)	21.6	3.2	-	45.5	18.5	11.2

(b)

Fig. 10 – SEM micrographs of the worn surface of the laser-alloyed specimen Cu–Cr–Ti-20%CNT P1.5V15: (a) low magnifcation and (b) high magnification.

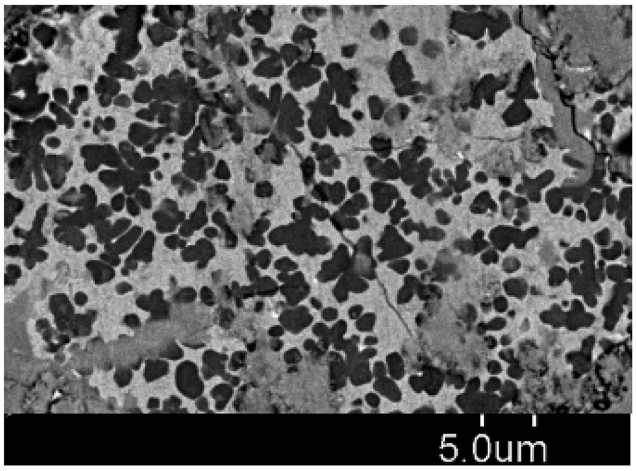

(a)

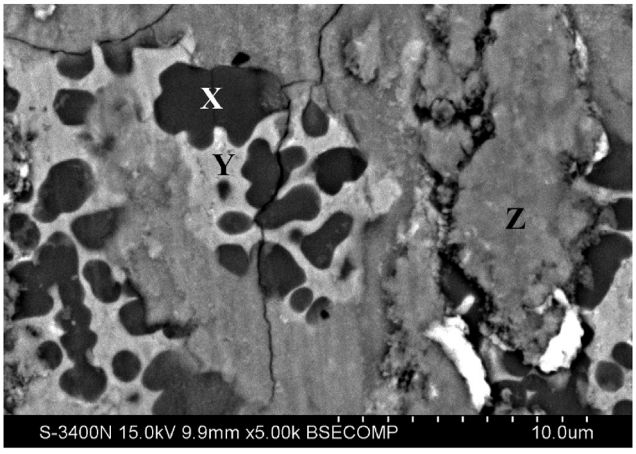

Composition (wt.%)	Ti	Cr	Fe	Cu	O	C
X (TiC)	78	5.5	-	-	-	16.5
Y (Cr-rich)	6.4	88.1	1.1	44.3	-	-
Z (Fe-rich)	6.5	6.9	83.6	3.0	-	-

(b)

Fig. 11 – SEM micrographs of the worn surface of the laser-alloyed specimen Cu–Cr–Ti-20%CNT P1.5V20: (a) low magnifcation and (b) high magnification.

factor 6.3) due to the presence of the passivable W phase in the NaCl solution [5]. It was also reported that the W phase of the W–Cu alloys was more active than the Cu phase and slowly dissolved initially in the neutral NaCl solution [40]. The corrosion resistance of W–Cu alloys was high because tungsten oxide existed and the Cu binder was cathodically protected. The Cu binder took part in the rapid anodic reaction and was selectively corroded as the potential increased. The corrosion rate of Cu was 100 times higher than that of W.

While the corrosion rate of the laser-alloyed Cu with Ti (25–85 wt%) decreased with the increase in Ti content in the 3.5 wt% NaCl solution [8]. Even though the laser-alloyed Cu with Ti also did not show significant passivity and thermodynamic stability was not as stable as cp Cu, their corrosion resistance is higher than that of cp Cu at most by a factor of 100 [8]. Due to the existence of the active IMPs, the oxide layer on the laser-alloyed Cu with Ti could not provide an effective barrier against corrosion. Similarly, the laser-alloyed Cu with NiTi also did not show considerable passivity in the 3.5 wt% NaCl solution [9]. Compared with NiTi, the oxide layers formed on the laser-alloyed Cu with NiTi were non-uniform and less stable for corrosion protection. The heterogeneity (i.e. IMPs/TiO_2) could lead to a defective passive film acting as the initiation sites for pitting attack [9]. A local breakdown of the oxide layer could begin due to preferable adsorption of the chloride ions on the surface and consequently oxide repassivation was hindered at such locations.

Akkaş and his co-workers [41] have investigated the corrosion behavior of Cu-xTiC (x = 0, 1, 5, 10 and 15 wt%)

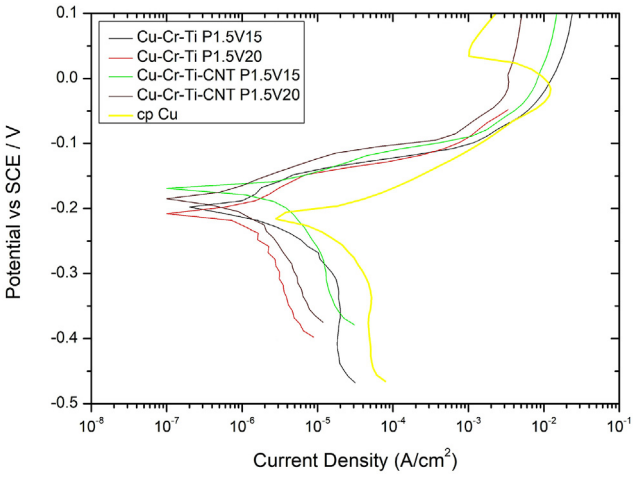

Fig. 12 – Potentiodynamic polarization curves of laser-alloyed specimens and cp Cu in 3.5 wt.% NaCl solution at 25 °C.

composites fabricated by hot pressing. The corrosion potential of the unreinforced Cu (−0.21 V) was the noblest and the I_{corr} was the lowest (6 μA/cm^2). While corrosion potential for Cu with 15 wt% TiC was found to be the most active (−0.242 V) and the I_{corr} is the highest (43.7 μA/cm^2). As the TiC content in the Cu-matrix increased, the corrosion resistance of the composite decreased because the higher porosity content in the composite facilitated corrosion attack [41]. In the present study, 20.4 vol% and 60.5 vol% TiC were present in the Cu-matrix of Cu–Cr–Ti-20%CNT P1.5V15 and the Cr-matrix of Cu–Cr–Ti-20%CNT P1.5V20 respectively. The corrosion potential of Cu–Cr–Ti-20%CNT P1.5V15 (−0.170 ± 0.001 V_{SCE}) is slightly nobler than that of Cu–Cr–Ti-20%CNT P1.5V20 (−0.185 ± 0.002 V_{SCE}) as Cu is the major phase of the former. While the I_{corr} of Cu–Cr–Ti-20%CNT P1.5V15 (0.164 ± 0.005 μA/cm^2) with lower TiC content was found to be lower than that of Cu–Cr–Ti-20%CNT P1.5V20 (0.170 ± 0.007 μA/cm^2) with higher TiC content. The present finding is consistent with that of Akkas's group, i.e. higher the TiC content, lower the corrosion resistance of the specimen. Compared with the Cu-*x*TiC composites obtained by hot pressing [39], the I_{corr} of the laser-alloyed specimens with CNT (with much higher TiC content in the Cr/Cu-matrix) are much lower because porosity is absent.

4. Conclusions

The present work was devoted to the study of laser surface alloying of cp Cu with Cr/Ti and Cr/Ti/CNT for improving hardness, wear and corrosion resistances. The main findings of this study are concluded below:

1. Cu, Cr, Cu_3Ti, Cu_3Ti_2, Cu_4Ti_3 were detected in the laser-alloyed specimens without CNT. While Cr, Cu and TiC were found in the laser-alloyed specimens with CNT.
2. Compared with cp Cu (60 ± 10 $HV_{0.2}$), the laser-alloyed specimens without and with CNT could achieve hardness up to 423 ± 12 $HV_{0.2}$ and 860 ± 24 $HV_{0.2}$ respectively.
3. Compared with cp Cu, the wear resistance of all laser-alloyed specimens were significantly improved due to solid solution alloying, and existence of the hard phases including Cr, Cu–Ti intermetallic phases and TiC. The wear resistance of the laser-alloyed specimen with CNT is enhanced by a factor of 1220.
4. The corrosion current densities of all laser-alloyed specimens in 3.5 wt% NaCl solution at 25 °C (0.164–0.275 μA/cm^2) are found to be lower than that of cp Cu (3.362 μA/cm^2) by an order of magnitude due to presence of passive elements (Cr and Ti).

Declaration of Competing Interest

The authors declare that they have no known competing financial interests or personal relationships that could have appeared to influence the work reported in this paper.

Acknowledgments

This work was supported by the Science and Technology Development Fund from Macau SAR [Grant number 0139/2020/A3], Multi-Year Research Grant (MYRG) of University of Macau [Grant number MYRG2018-00217-FST] and the Institute for the Development and Quality, Macau.

REFERENCES

[1] Draper W, Poate JM. Laser surface alloying. Int Met Rev 1985;30:85–108.
[2] Kwok CT, Man HC, Cheng FT, Lo KH. Developments in laser-based surface engineering processes: with particular reference to protection against cavitation erosion. Surf Coating Technol 2016;291:89–204.
[3] Hirose A, Kobayashi KF. Surface alloying of copper with chromium by CO_2 laser. Mater Sci Eng, A 1994;174:174–99.
[4] Pelletier JM, Issa A, Fouquet E. Possibilities and limitations of laser surface alloying by melting of predeposited layers. J Phys IV 1991;1:87–90. C7.
[5] Wong PK, Kwok CT, Man HC, Guo D. Laser fabrication of W-reinforced Cu layers: I. Corrosion behavior in 3.5% NaCl solution and synthetic acid rain. Mater Chem Phys 2016;181:397–408.
[6] Wong PK, Kwok CT, Man HC, Guo D. Laser fabrication of W-reinforced Cu layers: II. Electrical wear behavior in air and synthetic acid rain. Mater Chem Phys 2016;177:118–30.
[7] Kwok CT, Wong PK, Man HC. Laser surface alloying of copper with titanium: Part I. Electrical wear resistance in dry condition, and Laser surface alloying of copper with titanium: Part II. Electrical wear resistance in wet and corrosive condition. Surf Coating Technol 2016;29:66–73.
[8] Wong PK, Kwok CT, Man HC, Cheng FT. Corrosion behavior of laser-alloyed copper with titanium fabricated by high power diode laser. Corrosion Sci 2012;57:228–40.
[9] Kwok CT, Wong PK, Man HC. Enhancement in corrosion and electrical wear resistance of copper via laser surface alloying with NiTi. Surf Coating Technol 2021;408:126804.
[10] Wong PK. Laser surface modification of copper for corrosion and electrical wear resistance. 2016. p. 239. PhD Dissertation.
[11] Markandeya R, Nagarjunab S, Sarma DS. Precipitation hardening of Cu-Ti-Cr alloys. Mater Sci Eng 2004;371:291–305.

[12] Sun Z, Guo J, Li Y, Zhu Y, Li Q, Song X. Effects of Ti addition on the liquid-phase separation of $Cu_{71}Cr_{29}$ alloy during rapid cooling. Metall Mater Trans 2008;39A:1054–9.
[13] Chen K, Zeng L, Li Z, Chai L, Wang Y, Chen LY, et al. Effects of laser surface alloying with Cr on microstructure and hardness of commercial purity Zr. J Alloys Compd 2019;784:1106–12.
[14] Wang T, Zeng L, Li Z, Chai L, Cheng T, Zhang L, et al. Influences of laser surface alloying with Cr on microstructural characteristics and hardness of pure Ti. Metall Mater Trans 2019;50:3794–804.
[15] Man HC, Zhang S, Cheng FT, Yue TM. In situ synthesis of TiC reinforced surface MMC on Al6061 by laser surface alloying. Scripta Mater 2002;46:229–34.
[16] Savalani MM, Ng CC, Li QH, Man HC. In situ formation of titanium carbide using titanium and carbon-nanotube powders by laser cladding. Appl Surf Sci 2012;258:3173–7.
[17] Aboulkhaira NT, Marco S, Salamab E, Rancec GA, Neatec NC, Tucka Cal MK, et al. Evolution of carbon nanotubes and their metallurgical reactions in Al-based composites in response to laser irradiation during selective laser melting. Mater Sci Eng, A 2019;765:138307.
[18] Sadeghia N, Aghajanib H, Akbarpour MR. Microstructure and tribological properties of in-situ TiC-C/Cu nanocomposites synthesized using different carbon sources (graphite, carbon nanotube and graphene) in the Cu-Ti-C system. Ceram Int 2018;44:22059–67.
[19] Qiu F, Han Y, Cheng A, Lu J, Jiang Q. Effect of Cr content on the compression properties and abrasive wear behavior of the high-volume fraction (TiC–TiB_2)/Cu, composites. Acta Metall Sin 2014;27:951–6.
[20] Majumdar JD, Manna I. Laser surface alloying of copper with chromium I. Microstructural evolution. Mater Sci Eng, A 1999;268:216–26.
[21] Majumdar JD, Manna I. Laser surface alloying of copper with chromium II. Improvement in mechanical properties. Mater Sci Eng, A 1999;268:227–35.
[22] Dehm G, Medres B, Shepeleva L, Scheu C, Bamberger M, Mordike BL, et al. Microstructure and tribological properties of Ni-based claddings on Cu substrate. Wear 1999;225–229:18–26.
[23] Pelletier JM, Issa A, Sallamand P. Laser surface alloying on copper base alloys. Laser Eng 1993;2:81–92.
[24] Jendrzejewski R, Sliwinski G. Investigation of temperature and stress fields in laser cladded coating. Appl Surf Sci 2007;254:921–5.
[25] ASTM standard G5-92: 'standard reference test method for making potentiodynamic anodic polarization measurement. Philadelphia: ASTM Standards; 1994.
[26] Ion JC. Laser processing of engineering materials: principles, procedure and industrial application. Oxford: Elsevier Butterworth-Heinemann; 2005. p. 219.
[27] Wang LZ, Chen T, Wang S. Microstructural characteristics and mechanical properties of carbon nanotube reinforced AlSi10Mg composites fabricated by selective laser melting. Optik 2017;143:173–9.
[28] Kimura Y, Kaito C. Formation of carbon nanotubes from mixture film of carbon and titanium. Phys E Low-dimens Syst Nanostruct 2005;28:281–5.
[29] Pelaprat JM, Finu M, Fritz R, Zediker M. Laser focus world, novel lasers: blue direct-diode lasers extend industrial laser capability. 2018. https://www.laserfocusworld.com/lasers-sources/article/16555269/novel-lasers-blue-directdiode-lasers-extend-industrial-laser-capability.
[30] Paquin R. Properties of metals. In: Bass M, Stryland EW, Williams DR, Wolfe WL, editors. Handbook of optics, volume II: devices, measurements, and properties. 2nd ed., vol. 35. McGraw-Hil; 1995. p. 32.
[31] Lehman J, Varaksa N, Theocharous T, Dillon A. Carbon nanotube-based coatings for laser power and energy measurements. Laser Microfabrication Conference ICALEO 2005 Congress Proceedings 2005:344–8. Paper #M703.
[32] Zhang K, Stocks GM, Zhong J. Melting and premelting of carbon nanotubes. Nanotechnology 2007;18:285703.
[33] Pitroda J, Jethwa B, Dave SK. A critical review on carbon nanotubes. International Journal of Constructive Research in Civil Engineering 2016;2:36–42.
[34] Gao F, Wang HM. Dry sliding wear property of a laser melting/deposited Ti_2Ni/TiNi intermetallic alloy. Intermetallics 2008;16:202–8.
[35] Bateni MR, Asrafizadeh F, Szpunar JA, Drew RAL. Improving the tribological behavior of copper through novel Ti-Cu intermetallics coatings. Wear 2002;253:626–39.
[36] Bagheri GHA. The effect of reinforcement percentages on properties of copper matrix composites reinforced with TiC particles. J Alloys Compd 2016;676:120–6.
[37] Colaço R, Vilar R. Abrasive wear of metallic matrix reinforced materials. Wear 2003;255:643–50.
[38] Xu T, Chen L, Chen Y, Yu SX, Liu B, Liu JH. Trans Nonferrous Metals Soc China 2004;14:520–4.
[39] Yu CY, Chang LM, Zhou LM, Lin HY. Trans Nonferrous Metals Soc China 2006;16:229–33.
[40] Guo D, Kwok CT. A corrosion study on W-Cu alloys in sodium chloride solution at different pH. J Mater Sci Technol 2021;64:38–56.
[41] Akkaş M, Islak S, Özorak C. Corrosion and wear properties of Cu-TiC composites produced by hot pressing technique. Celal Bayar University Journal of Science 2018;14:465–9.